Title

SUMOylation controls stem cell proliferation and regional cell death through Hedgehog signaling in planarians.

Journal

Cellular and molecular life sciences : CMLS, 75(7)

ISSN

1420-682X

Authors

Thiruvalluvan, Manish
Barghouth, Paul G
Tsur, Assaf
et al.

Publication Date

2018-04-01

DOI

10.1007/s00018-017-2697-4

Peer reviewed

Cell. Mol. Life Sci. (2018) 75:1285–1301
https://doi.org/10.1007/s00018-017-2697-4

Cellular and Molecular Life Sciences

ORIGINAL ARTICLE

SUMOylation controls stem cell proliferation and regional cell death through Hedgehog signaling in planarians

Manish Thiruvalluvan[1,2] · Paul G. Barghouth[1,2] · Assaf Tsur[3] · Limor Broday[3] · Néstor J. Oviedo[1,2,4]

Received: 1 September 2017 / Revised: 21 October 2017 / Accepted: 24 October 2017 / Published online: 2 November 2017

Abstract Mechanisms underlying anteroposterior body axis differences during adult tissue maintenance and regeneration are poorly understood. Here, we identify that post-translational modifications through the SUMO (Small Ubiquitin-like Modifier) machinery are evolutionarily conserved in the Lophotrocozoan *Schmidtea mediterranea*. Disruption of SUMOylation in adult animals by RNA-interference of the only SUMO E2 conjugating enzyme *Ubc9* leads to a systemic increase in DNA damage and a remarkable regional defect characterized by increased cell death and loss of the posterior half of the body. We identified that *Ubc9* is mainly expressed in planarian stem cells (neoblasts) but it is also transcribed in differentiated cells including neurons. Regeneration in *Ubc9*(*RNAi*) animals is impaired and associated with low neoblast proliferation. We present evidence indicating that *Ubc9*-induced regional cell death is preceded by alterations in transcription and spatial expression of repressors and activators of the Hedgehog signaling pathway. Our results demonstrate that SUMOylation acts as a regional-specific cue to regulate cell fate during tissue renewal and regeneration.

Keywords Ubc9 · Regeneration · Genomic instability · Rad51 · Patched

Introduction

The planarian *Schmidtea mediterranea* provides unique opportunities to dissect mechanisms controlling cellular decisions in the adult body. Signals influencing cellular behavior during adult tissue maintenance, repair, and cancer are evolutionarily conserved between planaria and mammals [2–8]. Systemic disruption of homologous recombination in *S. mediterranea* leads to dramatic increases in DNA double-strand breaks (DSBs) throughout the body [9]. Intriguingly, cells in the anterior region of the body survive and continue dividing with DSBs, while most cells in the posterior region of the planarian body undergo cell death. Brain signals and the retinoblastoma pathway contribute to the survival of cells with DNA damage in the anterior region [9]. However, it remains elusive which mechanisms operate in the posterior region, where cells with DSB are collectively eliminated by apoptosis.

To better understand mechanism(s) leading to collective cellular death, we searched for phenotypes involving regional defects across different animals. Disruption of the SUMOylation pathway during embryonic development in Drosophila and zebrafish lead to AP axis abnormalities and regional defects associated with cell death [10–12]. SUMOylation is an evolutionarily conserved post-translational modification that regulates a myriad of proteins and cellular processes including chromatin organization, transcription, DNA repair, apoptosis, cell

Electronic supplementary material The online version of this article (http://doi.org/10.1007/s00018-017-2697-4) contains supplementary material, which is available to authorized users.

✉ Néstor J. Oviedo
noviedo2@ucmerced.edu

1 Department of Molecular and Cell Biology, University of California, 5200 North Lake Road, Merced, CA 95343, USA

2 Quantitative and Systems Biology Graduate Program, University of California, Merced, USA

3 Department of Cell and Developmental Biology, Sackler School of Medicine, Tel Aviv University, Tel Aviv, Israel

4 Health Sciences Research Institute, University of California, Merced, USA

cycle control, protein trafficking, and signal transduction [13–15]. SUMOylation is a highly dynamic and reversible process whereby the small ubiquitin-like modifier (SUMO) is attached to target proteins, acting as a molecular switch that quickly controls protein activity [13]. The SUMOylation cascade requires *Ubc9*, the sole E2 conjugating enzyme necessary for properly attaching SUMO to target proteins [16–20]. Inactivation of *Ubc9* is embryonically lethal, limiting our understanding about the role of SUMOylation in the maintenance and repair of adult tissues [10–12, 21].

Our present findings show that the SUMO pathway is evolutionarily and functionally conserved in the Lophotrocozoan *S. mediterranea*. Disruption of the SUMOylation pathway in planarians with RNA-interference of *Ubc9* lead to regional defects characterized by loss of the posterior half of the body (tail), systemic loss of the adult stem cells and increase in DNA damage, specifically DSBs. In addition, *Ubc9* is required for posterior specific tissue maintenance and regeneration through the regulation of the Hedgehog (Hh) pathway. Altogether, we propose that SUMOylation controls regional fate decisions by balancing activators and repressors of the Hh signaling.

Results

The SUMOylation pathway is conserved in the planarian *Schmidtea mediterranea*

The SUMOylation pathway is cyclic in nature and can be broadly summarized in five steps: SUMO maturation, activation, conjugation, attachment and its removal from the target protein (Fig. 1a). Components of the SUMOylation pathway are evolutionarily conserved from yeast through mammals [13]. The *S. mediterranea* genome includes homologs of all components of the general SUMOylation pathway (Fig. 1b). Interestingly, the two SUMO proteins we identified in planarians are the homologs of SUMO-2/3 and not SUMO-1 (Figure S1A, B). Consistent with other organisms, there is only one homolog for the SUMO E2 conjugating enzyme UBC9 (*Smed-Ubc9*, henceforth *Ubc9*). In most cases, *Ubc9* is known to be the linchpin controlling the SUMOylation pathway and acts as a rate-limiting step for SUMO conjugation [13]. Phylogenetic analysis of UBC9 across different phyla confirms its evolutionary conservation, which in the case of planarians is 73% identical to its human counterpart (Fig. 1c, S1C). These results suggest that the SUMO pathway is evolutionarily conserved in *S. mediterranea*, a Plathyhelmith member of the Lophotrocozoan clade.

SUMOylation is required for regional tissue maintenance

To functionally characterize the role of *Ubc9* in *S. mediterranea*, we performed RNA interference by feeding with dsRNA expressing bacteria mixed with liver six times every three days, and animals were fixed 25 days after the first dsRNA feeding (25 dpf) (Fig. 2a). Animals subjected to *Ubc9*(*RNAi*) exhibited macroscopic signs of tissue degradation, characterized by darkening of the epithelia in the post-pharyngeal region, followed by formation of lesions and complete loss of their tail by day 25 and onward (Fig. 2b). After 25 dpf, the experimental group undergoes rapid tissue deterioration and begins to lyse (Fig. 2c). We noticed that *Ubc9*(*RNAi*) animals have an apparent reduction in size before losing their tail, which was confirmed by the reduction in surface area that started 15 dpf (Fig. 2d). Despite the tissue loss being restricted to the posterior region, qPCR experiments revealed that *Ubc9* gene expression was effectively downregulated throughout the whole organism at 25 dpf (Fig. 2e).

Ubc9 is expressed in neoblasts and post-mitotic cells

To further understand *Ubc9* function in planarians, we characterized its spatial distribution with in situ hybridization and found it is ubiquitously expressed throughout the organism (Fig. 3a). Interestingly, *Ubc9* expression is dramatically reduced 24 h after lethal irradiation (6 k rads), which is known to eliminate planarian stem cells or neoblasts [22], and remains at that level 7 days post-irradiation (dpi) (Fig. 3a). In addition, we detected residual *Ubc9* expression surrounding the pharynx and the periphery of the brain at 7 dpi (Fig. 3a). Distribution of *Ubc9* expression among neoblasts and post-mitotic cells was further confirmed using the single-cell sequencing database [1] (Fig. 3b, c). Furthermore, the single-cell analysis also reveals that *Ubc9* expression is present across all neoblast subclasses and in a subset of differentiated cells including neural, epidermal, and gut (Fig. 3c, S2). Together, these findings suggest that *Ubc9* is mainly expressed in neoblasts but it is also transcribed in post-mitotic cells.

Ubc9 is required for the proper function of stem cells

Neoblasts are the only proliferative cells in planarians, and thus we evaluated mitotic activity by whole-mount immunostaining against phosphorylated histone-3 (H3P) at different time points after *Ubc9*(*RNAi*) (Fig. 3d). These experiments revealed a three-fold reduction in $H3P^+$ cells in the experimental group but residual mitotic activity remained (Fig. 3d, e). The macroscopic regional effects are visible by day 15 after *Ubc9*(*RNAi*) (Fig. 2c), but the mitotic decrease

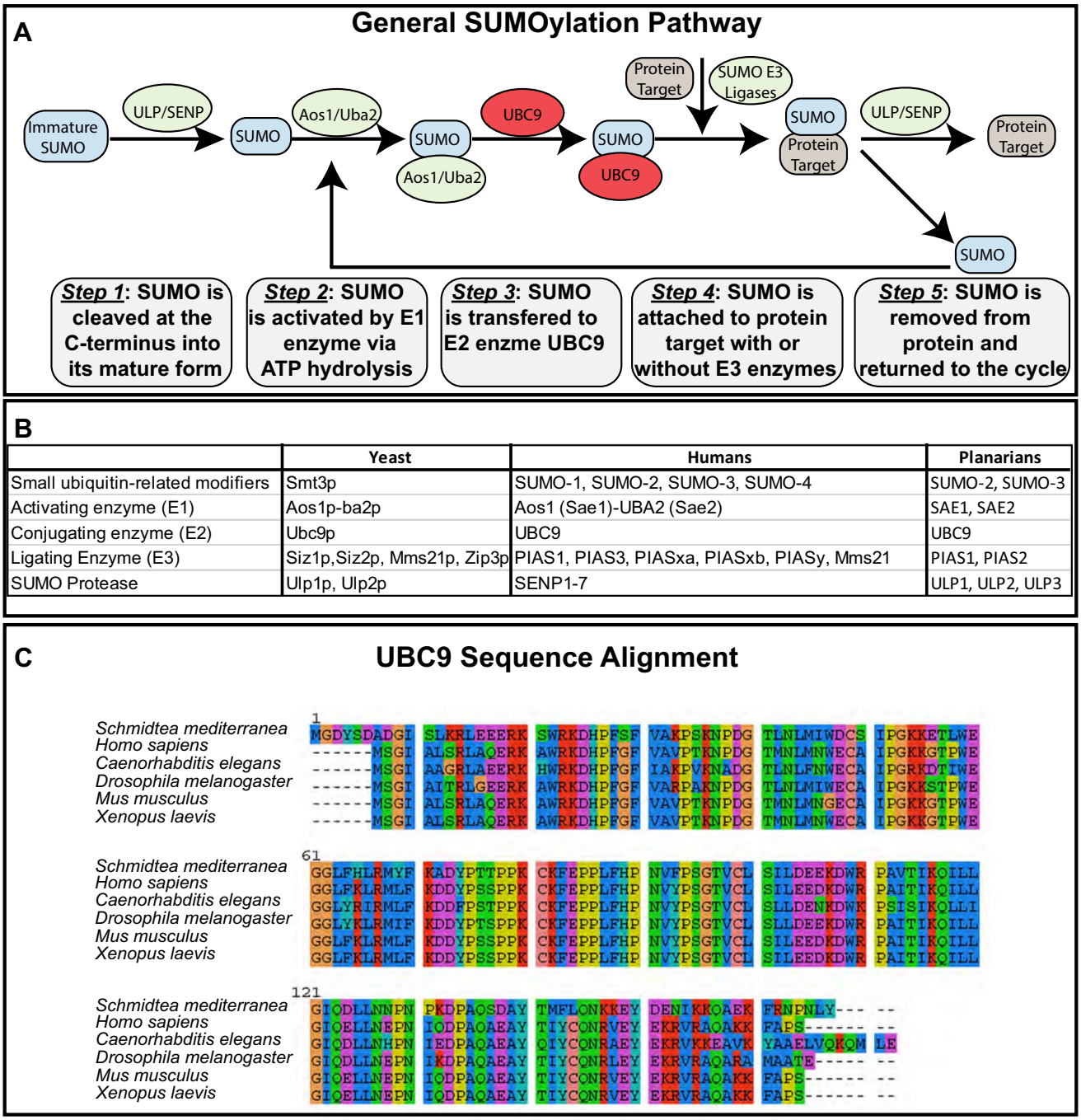

B

	Yeast	Humans	Planarians
Small ubiquitin-related modifiers	Smt3p	SUMO-1, SUMO-2, SUMO-3, SUMO-4	SUMO-2, SUMO-3
Activating enzyme (E1)	Aos1p-ba2p	Aos1 (Sae1)-UBA2 (Sae2)	SAE1, SAE2
Conjugating enzyme (E2)	Ubc9p	UBC9	UBC9
Ligating Enzyme (E3)	Siz1p,Siz2p, Mms21p, Zip3p	PIAS1, PIAS3, PIASxa, PIASxb, PIASy, Mms21	PIAS1, PIAS2
SUMO Protease	Ulp1p, Ulp2p	SENP1-7	ULP1, ULP2, ULP3

Fig. 1 The SUMOylation pathway is conserved in the planarian *Schmidtea mediterranea*. **a** A general outline of the SUMOylation pathway with the names of enzymes involved and a brief description of major steps in the process. **b** A list of SUMO pathway components found in humans and their homologs in yeast and *S. mediterranea*. **c** Protein alignment of planarian UBC9 and homologs found in humans (NP_003336.1), mice (EDL06246.1), *Drosophila* (NP_476978.1), *C. elegans* (NP_001023158.1) and *Xenopus* (NP_001080758.1). Human and planarian UBC9 protein sequences are 73% identical

is noted by day 20–25 post-RNAi. This suggests that tissue loss precedes effects in neoblast proliferation. To evaluate whether there was a regional reduction in mitotic activity, we separately quantified $H3P^{+}$ cells in the anterior and posterior regions. Each animal was split into two parts along the AP axis, considering the prepharyngeal as the anterior region and the remaining tissue including the pharynx as the posterior region (Fig. 2e). Such delimitation was made to account for the dramatic reduction in the tail region in the phenotype. This analysis demonstrated that loss of mitotic

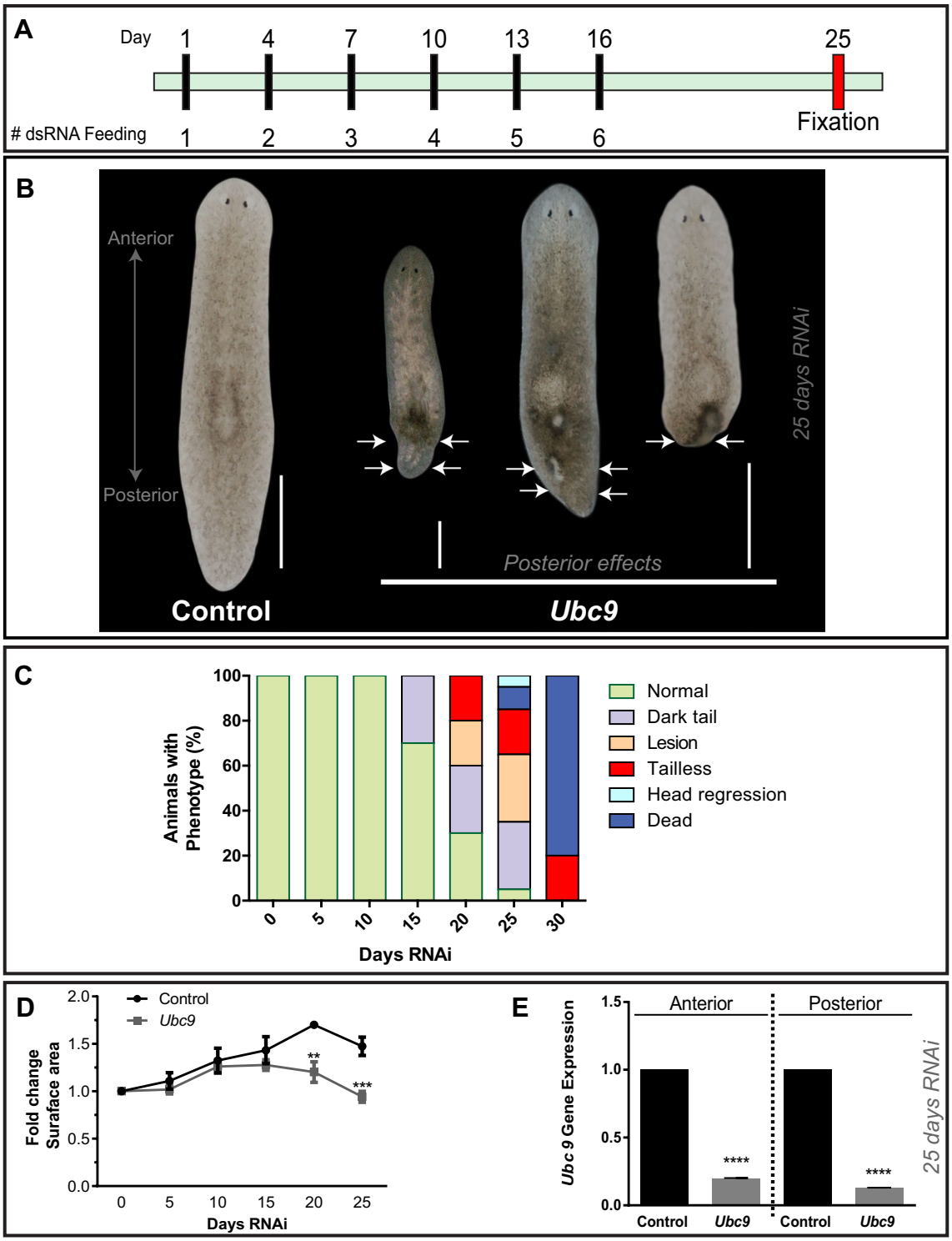

Fig. 2 *Ubc9* is required for regional tissue maintenance. **a** RNAi schedule based on feeding with bacterially expressed dsRNA to knockdown *Ubc9* expression. All controls were fed either *Unc22* or *gfp*. Black bars represent feeding days and red represents fixation. **b** Representative images of control and *Ubc9*(*RNAi*) animals 25 dpf. The arrows indicate different abnormalities including dark tail, lesions, and tail loss. $n = 75$ total animals used in three biological replicates. Scale bar = 200 µm. Note the scale bar on the right applies for the two pictures on the right portion of the figure. **c** Histogram illustrates the progression of the *Ubc9* phenotype based on macroscopic abnormalities observed in "**b**". **d** Change in surface area over the 25-day RNAi time course in controls and *Ubc9*(*RNAi*) animals. The experiment involves 15 animals per time point and three biological replicates. **e** Levels of *Ubc9* expression measured with qPCR. The results show that the RNAi knockdown protocol is effective at reducing transcript levels of *Ubc9* in both anterior and posterior regions. Data obtained from triplicates per experiment of at least two biological replicates. ****$p < 0.0001$; two-way ANOVA

activity was halved along both the anterior and the posterior regions (Fig. 3f).

Next, we analyzed the effects of *Ubc9* downregulation on cell populations and cell cycle dynamics using flow cytometry (FACS) [23]. Pooled cells from anterior and posterior regions were processed separately in both control and *Ubc9*(*RNAi*) animals 25 dpf. First, we examined cellular populations associated with neoblasts (X1) and early and late post-mitotic progeny (X2 and Xins, respectively) [23, 24]. There was an overall reduction in the proliferative X1 population across the AP axis, which was more noticeable (~ 4 fold) in the posterior region of the experimental group (Fig. 3g). The decline in the X1 cells is consistent with the reduction in mitotic activity (Fig. 3d–f). However, *Ubc9*(*RNAi*) has an unexpected increase on post-mitotic X2 cells in the anterior region, whereas the posterior region shows the expected decline (Fig. 3g). The mechanism behind this observation remains to be investigated.

Taken together, whole mount in situ hybridization and gene expression levels demonstrate that *Ubc9*(*RNAi*) lead to severe downregulation in markers of X1, X2 and Xins cells (*Smedwi-1*, *Smed-prog-1* and *Smed-AGAT-1,* respectively) (Figure S3A, B). Interestingly, the dramatic reduction in the expression of early progeny marker (*Smed-prog-1*) in the tail region and the persistence of some positive *Smed-prog-1* cells in the anterior region may imply that the enrichment of the X2 fraction is specific to the anterior region of *Ubc9*(*RNAi*) animals. Nonetheless, this finding demonstrates that *Ubc9* is required for the proper function of neoblasts and differentiated cells. Previous studies have shown that blockage in G1 phase of the cell cycle is observed in other organisms after *Ubc9* depletion [25–28]. Consistently, we found in planarians that *Ubc9*(*RNAi*) leads to an increase in G1 phase (74.1 vs 81.1) and a decrease in S and G2/M (13.9 vs 6.02) phases of the cell cycle along the AP axis (Fig. 3h). In addition, the expression levels of genes that are evolutionarily conserved and commonly associated with G1, S and G2/M transitions were significantly decreased ($p < 0.0001$ two-way ANOVA) in *Ubc9*(*RNAi*) animals (Fig. 3i). This is consistent with both a reduction in neoblast numbers and a concomitant reduction in cell cycle as observed in Figs. 3d–h. Together, these results suggest that *Ubc9* is required for maintenance of neoblasts and proper cell cycle transition.

Downregulation of SUMO proteins results in regional defects

We also tested whether RNAi of *S. mediterranea* SUMO proteins lead to gross morphological defects observed with *Ubc9*(*RNAi*). We identified two SUMO homologs in the *S. mediterranea* genome, which we termed *Smed-SUMO2* and *Smed-SUMO3* (Figure S1A, B). Individual RNAi of each component did not lead to behavioral or gross morphological defects, probably due to compensatory roles. However, double RNAi between the small ubiquitin-related modifiers *Smed-SUMO2* and *Smed-SUMO3* did produce regional defects like those noted after *Ubc9*(*RNAi*). Performing *Smed-SUMO2* + *SUMO3*(*RNAi*) led to accelerated tail loss in a fraction of the animals (i.e. 15% animals, 20 dpf) (Figure S4A). The remaining animals gradually underwent regional tissue loss and eventually died. Further evaluation of mitotic activity revealed that simultaneous downregulation of *Smed-SUMO2* + *SUMO3* dramatically reduced the number of proliferative cells across the animal (Figure S4B, C). Analysis of gene expression with markers for neoblasts and post-mitotic cells also demonstrated a dramatic decrease in expression that is consistent with the effects of *Ubc9*(*RNAi*) (Figure S4D). Collectively, these results suggest that regional defects and systemic neoblast dysfunction are specific to the disruption of SUMOylation through RNAi of *Ubc9* and/or *Smed-SUMO2* + *SUMO3*. For simplicity and consistency, we focused on analysis of the SUMO pathway through the downregulation of *Ubc9*.

Ubc9-systemic loss of function leads to regional cell death

To investigate the cause of regional tissue loss after *Ubc9*(*RNAi*), we analyzed cell death through whole-mount immunostaining and FACS [9, 23]. First, immunostaining assay with cell death marker caspase-3; which has been previously characterized in planarians [29], revealed an increase in cell death throughout the animal, with a prominent expression in the posterior region 25 dpf (Fig. 4a). In some instances, cell death signal was associated with cellular clusters, limiting our capacity to manually count dying cells. Instead, we chose to quantify the signal by generating an intensity profile of the fluorescence from anterior to posterior body axis. We found the intensity to be higher in *Ubc9*(*RNAi*), with a four time increase in cell death in the posterior region (Fig. 4b). *Ubc9*(*RNAi*)-induced cell death distribution was further analyzed by FACS using Annexin V, a marker of apoptosis that we have previously characterized in planarians [23]. Anterior and posterior fragments were processed separately and the results show that Annexin V^+cells are markedly increased in the posterior region of the experimental group (Fig. 4c). These results are consistent with regional cell death found in immunostaining using caspase-3 antibody. Furthermore, gene expression of *BCL2*, a survival signal marker [30], is importantly reduced in the posterior region when compared to the anterior region (Fig. 4d). Taken together, our findings demonstrate that *Ubc9* is essential to cellular survival and regional tissue maintenance.

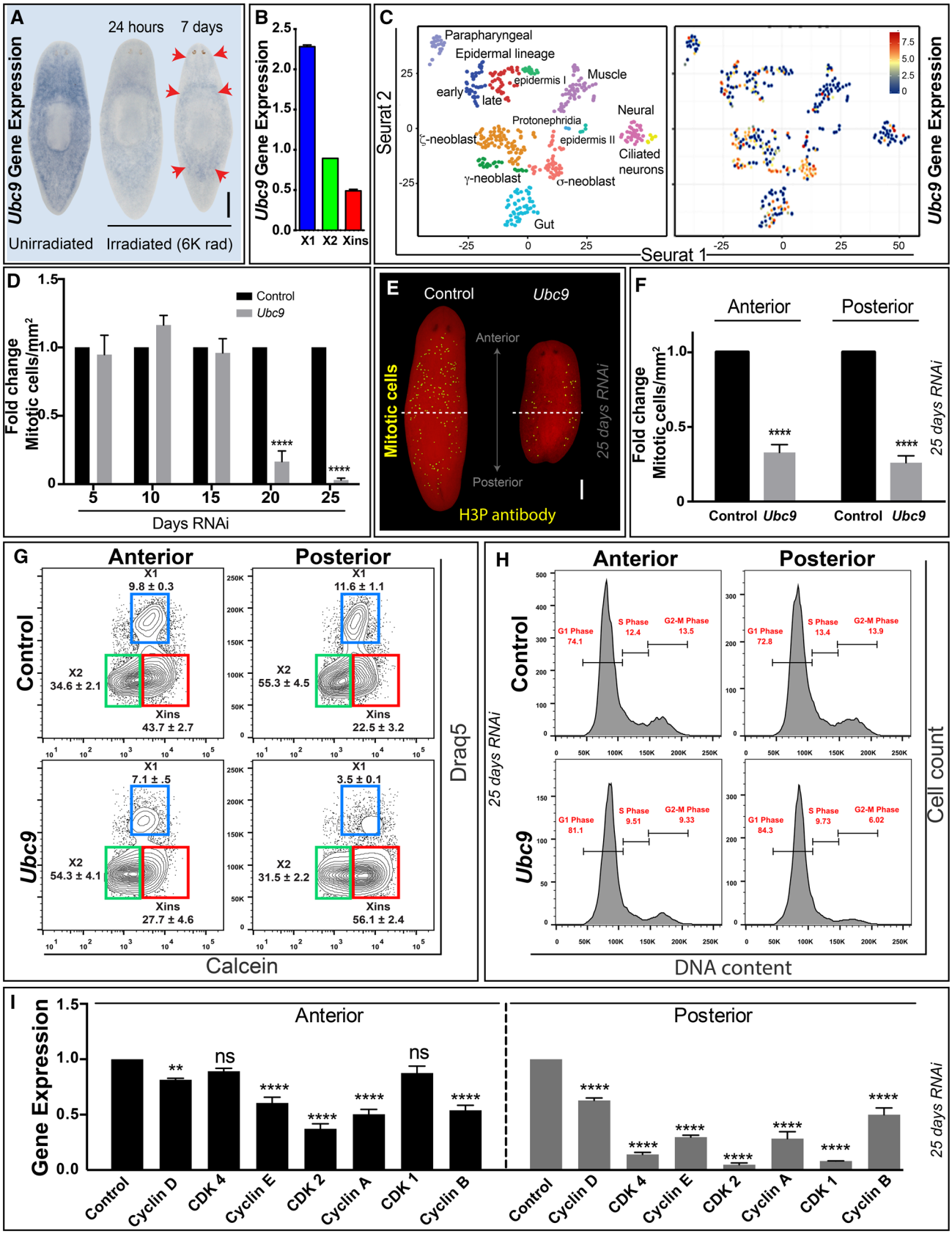
A
24 hours
7 days
Ubc9 Gene Expression
Unirradiated
Irradiated (6K rad)
B
Ubc9 Gene Expression
X1 X2 Xins
C
Parapharyngeal
Epidermal lineage
epidermis I
Muscle
early
late
Neural
Protonephridia
ζ-neoblast
epidermis II
Ciliated neurons
γ-neoblast
σ-neoblast
Gut
Seurat 2
Seurat 1
Ubc9 Gene Expression
D
Control
Ubc9
Fold change Mitotic cells/mm²
Days RNAi
E
Control
Ubc9
Anterior
Posterior
Mitotic cells
25 days RNAi
H3P antibody
F
Anterior
Posterior
Fold change Mitotic cells/mm²
Control Ubc9
Control Ubc9
25 days RNAi
G
Anterior
Posterior
Control
Ubc9
X1 9.8 ± 0.3
X2 34.6 ± 2.1
Xins 43.7 ± 2.7
X1 11.6 ± 1.1
X2 55.3 ± 4.5
Xins 22.5 ± 3.2
X1 7.1 ± .5
X2 54.3 ± 4.1
Xins 27.7 ± 4.6
X1 3.5 ± 0.1
X2 31.5 ± 2.2
Xins 56.1 ± 2.4
Draq5
Calcein
H
Anterior
Posterior
Control
Ubc9
G1 Phase 74.1
S Phase 12.4
G2-M Phase 13.5
G1 Phase 72.8
S Phase 13.4
G2-M Phase 13.9
G1 Phase 81.1
S Phase 9.51
G2-M Phase 9.33
G1 Phase 84.3
S Phase 9.73
G2-M Phase 6.02
25 days RNAi
Cell count
DNA content
I
Gene Expression
Anterior
Posterior
Control
Cyclin D
CDK 4
Cyclin E
CDK 2
Cyclin A
CDK 1
Cyclin B
25 days RNAi

◂**Fig. 3** *Ubc9* is necessary for stem cell function and proper cell cycle transition. **a** Whole mount in situ hybridization using antisense probe against *Ubc9*. Gene expression is found ubiquitously distributed along the AP axis (left) and is dramatically reduced 24 h after lethal exposure to gamma irradiation (6 K rads) and remained at that level for 7 days post-irradiation (red arrows). Experiments involved three biological replicates with 10 animals per experiment. **b** *Ubc9* gene expression levels in different cell populations (X1: proliferative cells, X2: early post-mitotic progeny, and Xins: late post-mitotic progeny). **c** t-SNE plot of single cells displaying clusters of neoblasts and differentiated cells (left), along with the overlaid *Ubc9* expression (right). The respective reference for the level of expression based on the colored gradient scale blue to red (low–high, respectively). The gene expression result for "**b** and **c**" were obtained from the planaria single-cell database hosted by the Reddien Lab at the Whitehead Institute for Biomedical Research (https://radiant.wi.mit.edu/app/) [1]. **d** Time course of mitotic activity along the AP axis, expressed as fold change in reference to the control at each time point. **e** Spatial distribution of mitotic activity in whole mount immunostaining against phospho-histone H3 (Ser10) (H3P) at 25 dpf *Ubc9*(*RNAi*). Dashed line divides anterior and posterior regions of the animal. All scale bars = 200 µm. **f** Fold change mitotic counts obtained independently from the anterior or posterior regions. Mitotic levels involved three biological replicates and more than 40 animals. **g** FACS analysis using DRAQ5, a nuclear dye and Calcein, a live cell marker, in either anterior or posterior regions of control and *Ubc9*(*RNAi*) animals 25 dpf. Blue, green and red squares represent X1, X2 and Xins populations, respectively. **h** Cell cycle analysis using DRAQ5 DNA dye in AP regions of control and *Ubc9*(*RNAi*) animals 25 dpf. Red bars represent percentage of cells at different phases of cell cycle. All FACS analysis performed with more than 10,000 cells and results are representative of three experiments with about 40 animals total. **i** Gene expression levels of various cell cycle markers necessary for proper G1/S and G2/M transition in AP regions of control and *Ubc9*(*RNAi*) animals 25 dpf. Gene expression portrayed as fold change normalized to control. $^{**}p < 0.01$; $^{***}p < 0.001$; $^{****}p < 0.0001$; two-way-ANOVA

Ubc9 is required to maintain genomic integrity along the anteroposterior axis

Ubc9 downregulation in planarians resembles regional features of the *Rad51* phenotype, which is characterized by an increase in DNA double stranded breaks (DSBs) throughout the body [9]. To assess DNA integrity in *Ubc9*(*RNAi*) animals, we collected cells at different dpf and performed (1) COMET assay, (2) karyotyping and (3) immunostaining against markers required for early DNA damage response and repair through homologous recombination (HR). COMET assay was adjusted to detect DSBs [9, 31] and our results confirmed an increase in DNA damage equally distributed along the AP axis and is present as early as 10 dpf (Fig. 5a). The presence of DSBs was accompanied by a two fold increase in chromosomal abnormalities detected by karyotyping (Fig. 5b). Deletions, fusions and dicentric chromosomes characterized the abnormalities that affected all four pairs of chromosomes of the asexual *S. mediterranea* CIW4 strain. The spatial distribution of DNA damage in planarians can be detected with whole mount immunostaining using antibodies against ϒH2Ax (Figure S5) [31] and RAD51 [9, 32]. Our results with these antibodies revealed an increased signal for both in the experimental group (Fig. 5c, d). Interestingly, increase in signal intensities for both antibodies were consistently displayed in clusters in the pre-pharyngeal and post-pharyngeal area for 70% of the animals (Fig. 5c, d). Western blot also confirmed the increase in RAD51 signal after *Ubc9*(*RNAi*) (Fig. 5e, f). Increase in ϒH2Ax and RAD51 levels suggest that the mechanism for sensing DNA damage is active after *Ubc9*(*RNAi*).

To repair DSBs, RAD51 must be translocated from the cytoplasm to the nucleus. Thus, we tested whether RAD51 translocation was compromised in *Ubc9*(*RNAi*) animals. Exposure to gamma irradiation induces DSBs, and RAD51 protein expression and nuclear translocation is at a maximum after 5 days post sub-lethal irradiation (1.25 K rads) [9]. Therefore, control and *Ubc9*(*RNAi*) animals were exposed to sub-lethal irradiation and the cells were harvested after 5 days to evaluate RAD51 sub-cellular location (Fig. 5g). This experiment showed that RAD51 nuclear localization was observed in most of the control cells (~ 80%) whereas smaller fraction of cells (31%) in the experimental group exhibited the same behavior (Fig. 5h). In summary, these data indicate that *Ubc9* functions in maintaining DNA integrity and regulating RAD51 localization are conserved also in *S. mediterranea*.

Regional defects in *Ubc9*(*RNAi*) animals are mediated through modulation of the Hedgehog pathway

Posterior identity in planarians is associated with proper regulation of the evolutionarily conserved Hedgehog (Hh) pathway [16, 33, 34]. Specifically, regional determination of the posterior tissue is established through *Patched* (*Ptc*)-mediated signaling of *Hh* [33, 34]. Hh signaling in planarians is required for ciliogenesis, regeneration [16, 33, 34] and more recently, it has been linked to neural and glial function [17, 35]. However, it is still unknown whether this pathway is necessary for regional information in uninjured animals. Hh signaling activity can be assayed by gene expression analysis of anterior and posterior polarity markers, secreted frizzled protein 1 (*sfrp1*) and frizzled-like protein 4 (*fz4*), respectively [34]. Strikingly, the expression of both *fz4* and *sfrp1* was dramatically altered in uninjured *Ubc9*(*RNAi*) animals, while it remained without change in the control group. The expression of *sfrp1* was elevated and appeared ectopically in the lateral and tail regions at day 10 when compared to control animals (Fig. 6a, red arrows). The pattern and level of expression of *srfp1* decreased to wild-type at day 15. Inversely, *fz4* appeared ectopically in the head and lateral cells at day 10 but was strongly elevated at day 15. Both mRNAs were downregulated when the tail phenotype became obvious (Fig. 6a). This suggests that the

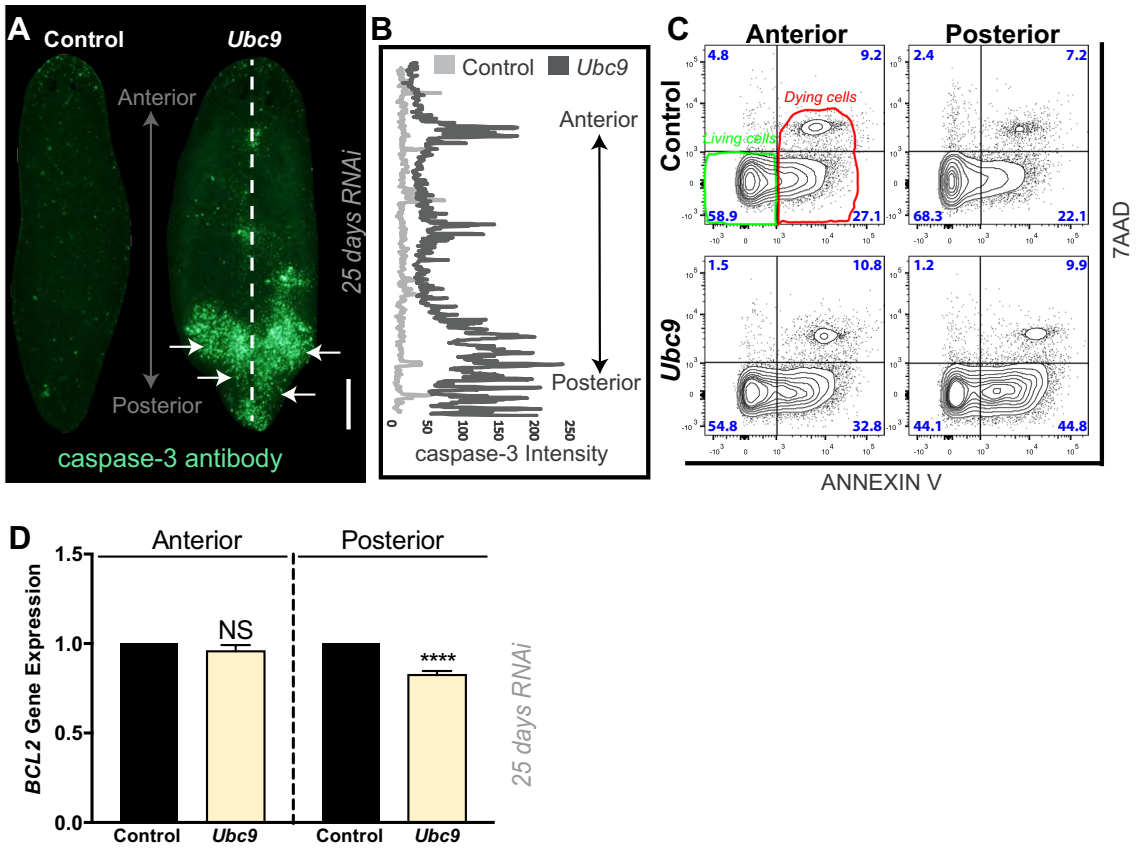

Fig. 4 *Ubc9*-loss of function leads to regional cell death. **a** Whole mount immunostaining against caspase-3, a marker for cell death, in control and *Ubc9*(*RNAi*) animals. About 65% of experimental animals showed similar caspase-3 signal distribution at 25 dpf. Immunostainings involved three biological replicates and more than 40 animals. Scale bars = 200 µm. **b** Intensity of capase-3 signal from anterior to posterior (white line) of control and *Ubc9*(*RNAi*) animals. Intensity signal quantification involved three biological replicates and more than 20 animals. **c** FACS analysis staining against Annexin V, a marker for apoptosis, and 7AAD, a cell viability marker, in AP regions of control and *Ubc9*(*RNAi*) animals 25 dpf. Annexin V-/7 AAD- quadrant includes viable cells (outlined green). Annexin V +/7 AAD– and Annexin V +/7 AAD + indicate cells that are in early and late (necrotic) stages of cell death, respectively (outlined red). Blue numbers in each quadrant indicate the percentage of cells with that staining profile. Data is representative of two experiments with $n > 40$ each. **d** Fold change of *BCL2* gene expression in anterior and posterior regions normalized to control group

downregulation of *Ubc9* may lead to transient ectopic activation of Hh signaling.

We next analyzed the expression of the inhibitor *Ptc* and activators *Hh* and *Smoothened* (*Smo*) at early and late phases of the *Ubc9* phenotype (i.e. 10, 15 and 25 dpf). *Ptc* expression shows a steady increase in days 15–25 that is more than double at late phases of the phenotype (Fig. 6b, c). *Hh* expression decreased at day 10 but increases at day 15 dpf and returned to basal levels at the late stage, while *Smo* expression appears stable. This suggests that depletion of *Ubc9* drives the pathway off equilibrium, leading to abnormal fluctuations in gene expression (Fig. 6b, c). To further examine the importance of the Hh pathway in mediating the loss of posterior homeostasis in *Ubc9*(*RNAi*) animals, we performed double RNAi experiments involving *Ptc*, *Hh*, and *Ubc9*. Different RNAi strategies were assayed and the most consistent results were obtained by first knocking-down either *Ptc* or *Hh* followed by *Ubc9* in a 40 days schedule that included a total of 14 feedings with dsRNA (Fig. 6d). Animals subjected to double RNAi *Ptc* + *Ubc9* displayed similar dynamics as in *Ubc9* alone (Figs. 2c, 6e). However, simultaneous downregulation of *Hh* + *Ubc9* led to more aggressive defects in the posterior region that appeared at day 10 and were lethal for 20% of the animals by day 20 of the *Ubc9*(*RNAi*) (Fig. 6e). The increased regional defects after *Hh* + *Ubc9*(*RNAi*), suggest synergistic/parallel contribution between these factors.

Sumoylation is required for planarian regeneration

We reasoned that if *Ubc9*(*RNAi*) leads to deregulation of the Hh pathway, then amputation would result in deficient tail and brain regeneration [33–35]. Control and *Ubc9*(*RNAi*) animals were amputated pre- and post-pharyngeally at 18

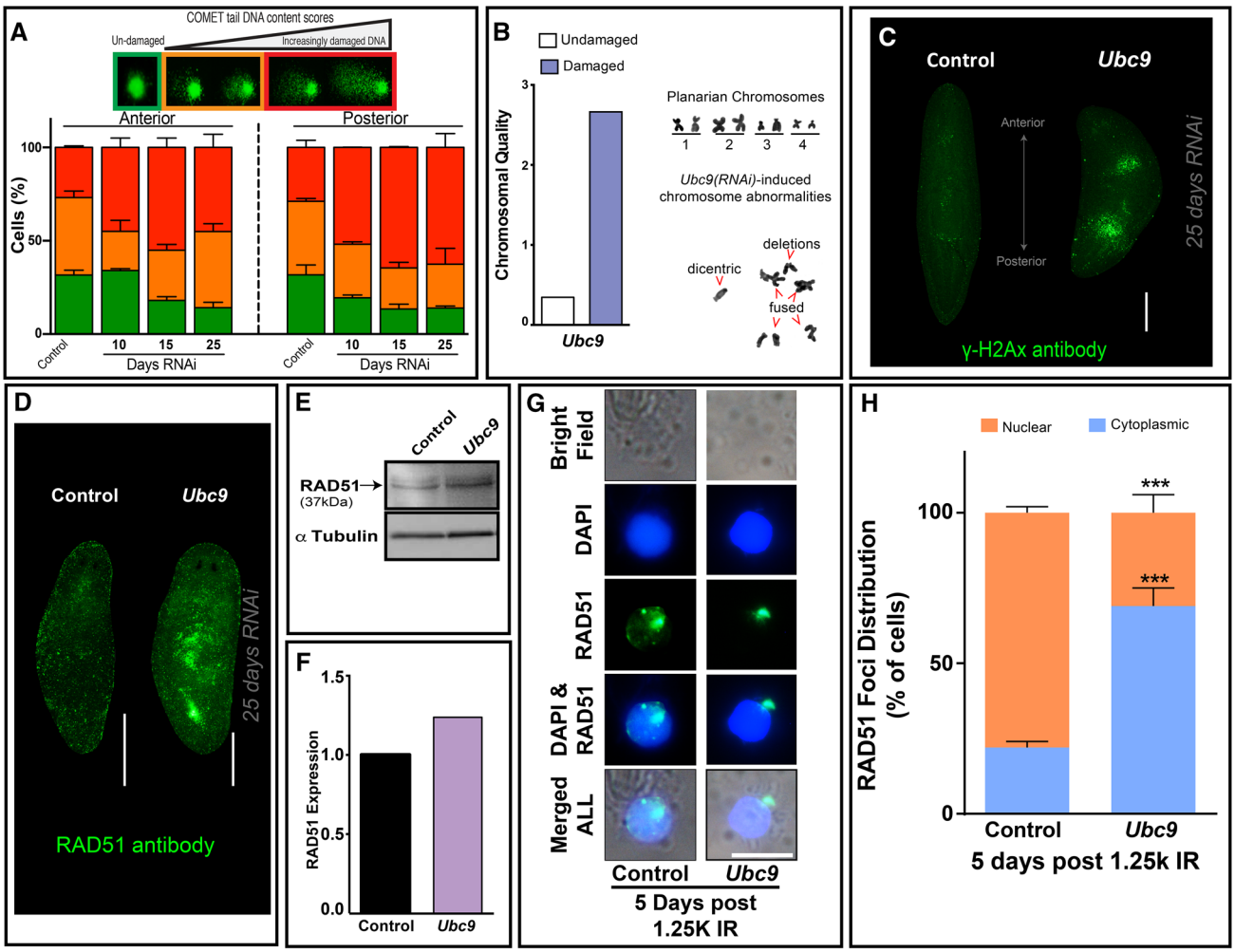

Fig. 5 *Ubc9* is required to maintain genomic integrity along the anteroposterior axis. **a** COMET assay, single gel electrophoresis under alkaline conditions, was performed in AP regions of control and *Ubc9*(*RNAi*) animals at10, 15, and 25 dpf. Visual scoring was used to quantify DNA damage. Color-coded key at bottom represents undamaged (green), moderate damage (orange) and extremely damaged DNA (red) shown in either anterior or posterior regions. DNA damage scale reference is similar to the one used in Peiris et al. 2016b. Downregulation of *Ubc9* leads to systemic accumulation of DNA damage as early as day 10 when compared to controls. Approximately 40 cells were counted for each DNA condition in two biological replicates. **b** Chromosome quality (not damage and damaged) normalized to control in *Ubc9*(*RNAi*) 25 dpf animals. Experiment was repeated twice. **c** Whole mount immunostaining against gamma H2AX antibody in control and *Ubc9*(*RNAi*) animals 25 dpf. Total number of animals was 20 and $n = 2$ biological replicates. **d** Whole mount immunostaining against human RAD51 antibody in control and *Ubc9*(*RNAi*) animals 25 dpf. Total number of animals was 15 and experiment was repeated twice. Scale bars = 200 µm and images are representative of approximately 70% of the animals in each condition. **e**, **f** Western-blot and subsequent quantification for RAD51 in control and *Ubc9*(*RNAi*) animals. Alpha tubulin was used as an internal control. Protein was extracted from $n > 30$ animals. **g** Spatial distribution of RAD51 immunostaining (green) in reference to the cell nucleus (stained with DAPI, blue) in control and *Ubc9*(*RNAi*) 18 dpf and 5 days after sub-lethal irradiation (1.25 k rads). RAD51 subcellular localization to the nucleus is at a maximum at this point in time. Scale bar = 10 µm. **h** Quantification of cells with RAD51 + foci in the nucleus and cytoplasm in control and *Ubc9*(*RNAi*) 18 dpf and 5 days after sub-lethal irradiation (1.25 k rads). Approximately 50 cells were counted for each condition in two biological replicates and all RAD51 stainings were performed with human RAD51 antibody

dpf, which is an early stage of the phenotype where most animals still retain posterior tissue but fluctuations in both *Ptc* expression and the downstream Hh components (*fz4* and *sfrp1*) are detected (Fig. 6b, c). Animals were then allowed to regenerate for 7 days (7 dpa) and blastema formation was evaluated (Fig. 7a). *Ubc9*(*RNAi*) animals formed small anterior blastemas and remarkably, lacked posterior blastema formation (Fig. 7b, c). To further examine the mechanism limiting regeneration, we assayed the mitotic response after amputation and revealed that *Ubc9*(*RNAi*) animals can sense injury, but respond with limited mitotic capability (Fig. 7d). Next, we considered whether regeneration of the nervous system was compromised after *Ubc9*(*RNAi*). Two main observations were made: (1) the size of the regenerated

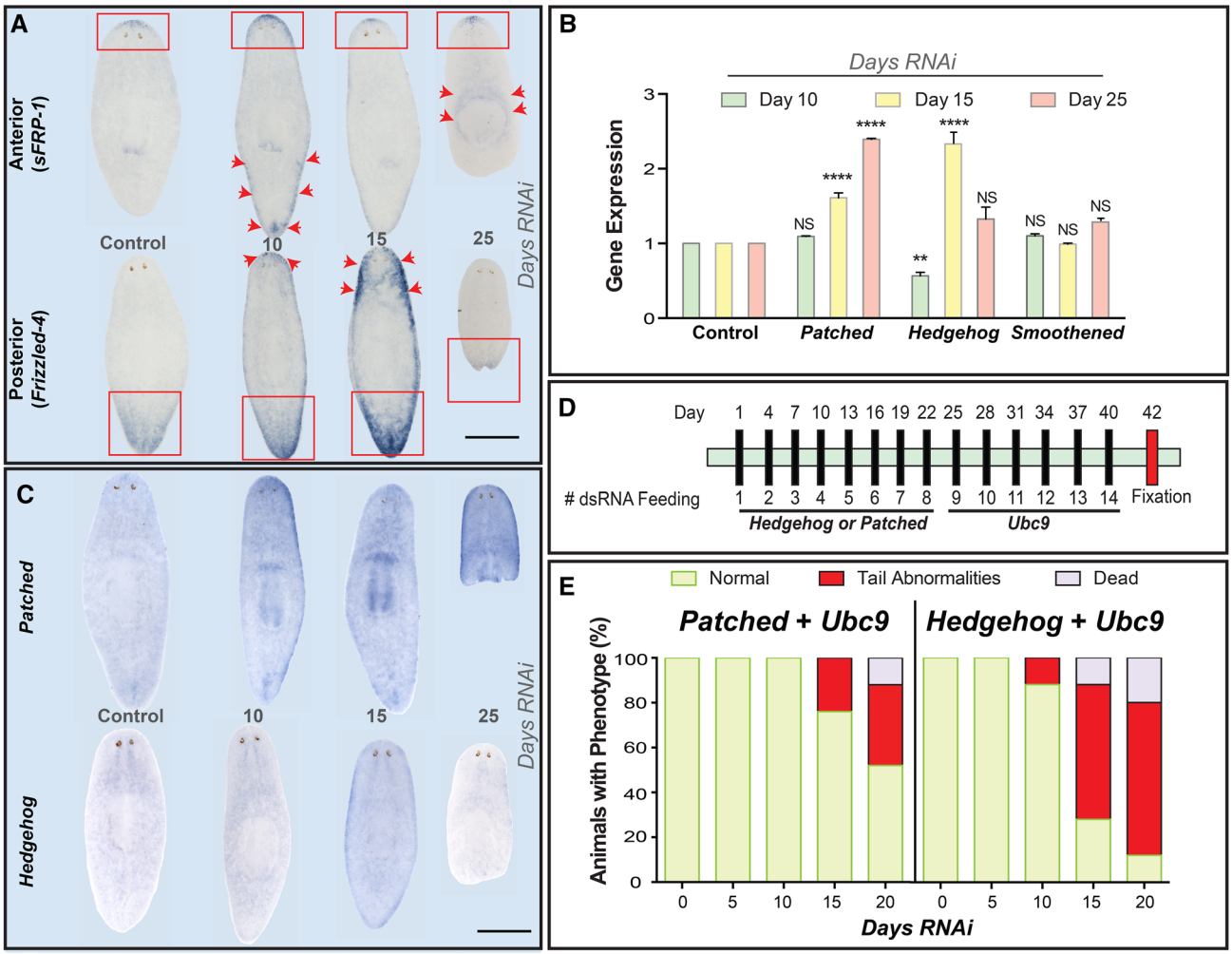

Fig. 6 Regional defects after *Ubc9*(*RNAi*) are mediated through repression of Hedgehog pathway. **a** Whole mount in situ hybridization expression of *sfrp-1* (anterior polarity marker) and *fz4* (posterior polarity marker) in control and 10, 15 and 25 dpf *Ubc9*(*RNAi*) animals. Red arrows indicate abnormal gene expression. Scale bars = 200 µm. Note that controls for each time point were executed but no apparent change in gene expression was observed over time –not shown. **b** Gene expression levels of *Patched*, *Hedgehog* and *Smoothened* after *Ubc9*(*RNAi*) animals at 10, 15 and 25 dpf. Gene expression is given in fold change normalized to control. **c** Whole mount in situ hybridization expression of *Patched* and *Hedgehog* in control and 10, 15 and 25 dpf *Ubc9*(*RNAi*) animals. Scale bars = 200 µm. **d**. RNAi schedule based on feeding with bacterially expressed dsRNA to perform double knockdown of *Hedgehog* or *Patched* and *Ubc9*. All controls were fed either *Unc22* or *gfp*. Black bars represent feeding days and red represents fixation. **e** Histogram depicts occurrence of tail abnormalities in *Hedgehog* + *Ubc9* and *Patched* + *Ubc9* animals. Data is representative of $n = 30$ animals consisting of three biological replicates

brain was reduced by half, consistent with compromised neurogenesis [35] (Fig. 7e, f) and (2) ventral nerve cords were truncated, likely due to the lack of posterior regeneration (Fig. 7e). Furthermore, we performed similar amputation experiments on double RNAi animals (Fig. 7g) and the regenerative outcome of these double knockdowns between *Ptc*, *Hh*, and *Ubc9* revealed that 100% of animals subjected to double RNAi *Ptc* + *Ubc9* and *Hh* + *Ubc9* presented lack of posterior blastema formation (Fig. 7h). This observation is in accordance with the posterior homeostasis synergistic/parallel effects (Fig. 6e). In addition, during regeneration, the anterior defects were more prevalent in the *Ptc* + *Ubc9*(*RNAi*) (over 90% of the animals), whereas 35% of the *Hh* + *Ubc9* showed regenerative defects in the anterior end as in single *Ubc9*(*RNAi*) (Fig. 7b). These results demonstrate that *Ubc9* is required for anterior and posterior blastema formation and organogenesis following injury.

Discussion

Regional signals contribute to cell fate decisions in the adult body. There is a tendency for cells in the anterior part of the body to have a superior proliferative response in health

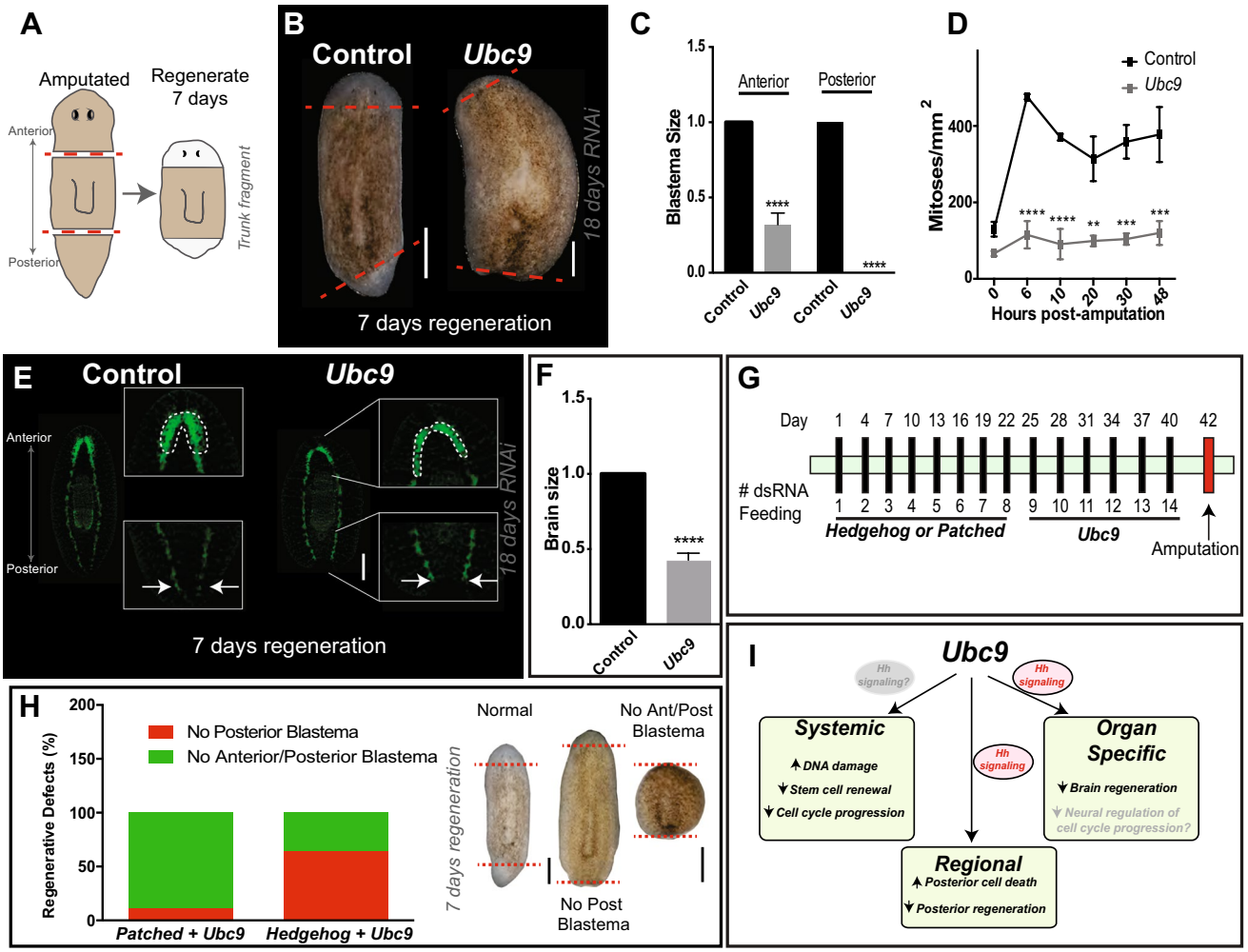

Fig. 7 *Ubc9* is required for proper regeneration. **a** Schematic representation of regeneration experiments on control and *Ubc9*(*RNAi*) animals 18 dpf. **b** Live pictures of control and *Ubc9*(*RNAi*) 18 dpf animals 7 days post amputation (7dpa). **c** Blastema size in control and *Ubc9*(*RNAi*) animals expressed as fold change relative to control. In all experiments used more than 30 animals in three biological replicates. **d** Trunk fragments generated from control and *Ubc9*(*RNAi*) 18dpf animals were fixed at 0, 6, 10, 20, 30 and 48 h post amputation. Mitotic cell numbers were determined via H3P staining and expressed as H3P + foci divided by surface area in mm^2. Three biological replicates with more than 15 animals per time point were used. **e** Whole mount immunostaining against SYNORF-1 (synapsin), a marker for the nervous system, in control and *Ubc9*(*RNAi*) 18 dpf 7DPA. Green signal denotes the planarian central nervous system and insets provide detailed amplification of anterior and posterior ends including brain and tip of the tail, respectively. White dotted lines underscore differences between control and experimental group regarding brain morphology (top) and ventral nerve cords (bottom). More than 20 animals were stained in three biological replicates. **f** Regenerated brain size obtained from determination of surface area in both control and experimental group. Differences in brain size were calculated with Two way-ANOVA. **g** RNAi schedule based on feeding with bacterially expressed dsRNA to perform double knockdown of *Hedgehog* or *Patched* and *Ubc9*. All controls were fed either *Unc22* or *gfp*. Black bars represent feeding days and red represents amputation. **h** Histogram depicts occurrence of regenerative defects in *Patched* + *Ubc9* and *Hedgehog* + *Ubc9* animals 7 days after amputation. Representative images of defects is shown on the right side. **i** Schematic summary representing *Smed-Ubc9* acts as an upstream regulator of different functions in the adult body. At the organismal level, downregulation of *Ubc9* lead to a systemic increase in DNA damage and decrease in in both stem cell renewal and cell cycle progression. However, it remains unclear whether inhibition of Hedgehog (Hh) signaling is associated with any of the systemic effects. Regionally, dysfunctional *Ubc9* triggers collective cell death and posterior specific abrogation of tissue regeneration, which are mediated through Hh signaling. At the organ level, *Ubc9* also regulates proper brain regeneration likely through disruption of Hh signaling that is required for neurogenesis. It is possible that lack of specific neurons in *Ubc9*(*RNAi*) animals also affect neural regulation of cell cycle progression but additional experiments are required. ****$p < 0.0001$ and all other statistical comparisons were made with Sidak's multiple comparisons test NS (no significance) $p > 0.05$; **$p < 0.01$; ***$p < 0.001$; ****$p < 0.0001$. Scale bars = 200 µm

and disease [36]. However, the mechanism underlying this regional difference remains poorly understood. Our results provide critical insight on the regulation of regional cell fate during tissue renewal and regeneration. Specifically, we demonstrate that the sole E2 conjugating enzyme *Ubc9*, an essential component of the SUMOylation pathway, controls cell cycle, stem cell renewal, adult tissue homeostasis and regeneration. In addition, *Ubc9* function is critical for subcellular translocation of RAD51 into the nucleus to repair DNA damage through homologous recombination. Finally, we establish *Ubc9* is an upstream regulator that exerts control over Hedgehog signaling to mediate regional cell fate decisions during tissue homeostasis and regeneration (Fig. 7i).

Post-translational modification (PTMs) with small ubiquitin-like modifier (SUMO) is a key regulator of various cellular processes in metazoans [13, 15]. We establish that SUMOylation is evolutionarily conserved in *S. mediterranea,* a member of the under studied group of Lophotrochozoans. This finding is critical because non-Ecdysozoan protostomes include the largest number of animal phyla across metazoans and the study of members of this group will complement, at the very least, information obtained in more traditional experimental organisms [37–39]. The lack of redundancy of *Ubc9* in the planarian genome recapitulates its evolutionarily conservation in the regulation of the SUMO pathway across eukaryotes. This is further evidenced by the close relationship in the protein sequence between human and planarian UBC9. A major challenge facing the study of *Ubc9* is the fact that its complete abrogation is embryonically lethal, which hampers our capacity to understand the systemic contribution of SUMO pathway at post-embryonic stages [40, 41]. Studies in *S. mediterranea* will provide unique opportunities to analyze PTMs through SUMOylation during simultaneous renewal of many tissues and regeneration in the context of the adult body.

The role of *Ubc9* in regulating stem cells depends on the context and the experimental models in which the studies are performed [42–45]. For example, *Ubc9* function is required for embryonic stem cell survival in vitro and reprogramming of induced pluripotent cells (iPS) but *Ubc9* function is not pertinent to the maintenance of mouse embryonic fibroblasts (MEFs) [46]. Our analysis looks at the function of *Ubc9* in planarians, which contain large pools of adult pluripotent stem cells (neoblasts). *Ubc9*(*RNAi*) led to rapid depletion of neoblasts across the AP body axis. This may be due to its effect on the cell cycle dynamics as knockdown of *Ubc9* causes an accumulation of cells in G1 phase and a reduction in G2/M phase. Previous studies have suggested knockdown of *Ubc9* is a key regulator of G1/S phase transition through various mechanisms of action [25, 28, 42, 44]. Additional findings suggest *Ubc9* knockdown induces DNA damage and chromosomal abnormalities, which would block cells from passing the critical cell cycle checkpoints [21, 47–49]. Therefore, this blockage in G1 phase could also impair the progression of post-mitotic progeny that will negatively impact the maintenance of differentiated tissues. Our findings in planarians are consistent with these observations and support a conserved role for SUMOylation in cell cycle control and adult stem cell maintenance.

Collective regulation of cellular decisions along the AP axis is subject to mechanisms that remain poorly understood. Earlier studies have demonstrated that downregulation of *Ubc9* induces regional cell death that precede lethality during embryonic development in *Drosophila* and zebrafish [10, 11]. In accordance, our results demonstrate consistent regional cell death followed by lethality, supporting functional conservation across metazoans and developmental stages. We propose that *Ubc9* functions as a regulator of regional cell death that prevails during embryonic development and adult stages.

Recently, we reported that loss of function of *Rad51*, a protein required for DNA repair through HR, induces regional defects in planarians [9]. *Ubc9*-mediated regional cell death follows a similar pattern as in *Rad51*(*RNAi*). Double RNAi experiments involving *Rad51* and *Ubc9* demonstrate a synergistic effect in reducing mitotic activity throughout the animal (Figure S6A, B). Furthermore, this complementary effect is also supported by the observation that each gene's expression is reduced but not completely abrogated after *Rad51* or *Ubc9*(*RNAi*) (Figure S6C, D). Taken together, these results suggest that the SUMO pathway overlaps with *Rad51* in some functions as RAD51 is probably also a SUMO target also in planarian, but still exert mitotic control through different mechanisms. For example, signals from the nervous system contribute to maintain mitotic activity in the anterior region of *Rad51*(*RNAi*) animals [9], whereas these neural inputs are limited after *Ubc9*(*RNAi*). It is possible that inhibition of the Hh pathway through *Ubc9* loss of function affects the neuronal subtype(s) [[35] and see discussion below] that send survival signals after abrogation of *Rad51*. However, the specific molecular mechanisms regulating anterior cellular fate in *Ubc9* animals remain to be investigated.

Downregulation of *Ubc9* leads to an increase in DSBs that are similarly distributed along the AP axis. Chromosomal abnormalities were also evident after *Ubc9*(*RNAi*), which is consistent with both defective DNA repair response and chromosomal segregation [21, 47–49]. We also noted that *Ubc9* downregulation leads to DNA damage response that occurs in clusters in both anterior and posterior regions, suggesting there may be focus of cells that are more susceptible to accumulate DSB. Future experiments will address the cause of DNA damage response in clusters after *Ubc9*(*RNAi*). Mechanistically, our results demonstrate that the increase in DSBs after *Ubc9*(*RNAi*) are due to a

disruption in DNA repair through HR. *Ubc9*(*RNAi*) restricts nuclear translocation of RAD51, which is consistent with previous studies showing UBC9 is involved in trafficking of nuclear proteins [21, 50–54]. These data together reveal *Ubc9* is an essential component to maintain genomic integrity during renewal of adult tissues.

The Ubc9 phenotype displays some resemblances in intact and regenerating animals. Specifically, during homeostasis, *Ubc9*(*RNAi*) animals lose their tail and during regeneration, worms are unable to form posterior blastema. In the anterior region, we show (Fig. 2c) that intact animals develop anterior abnormalities over time, which leads to loss of tissue in the anterior region but only at very late stages of the phenotype when they start dying (> 25 days post-RNAi). The regenerating worms also show defective anterior regeneration that is associated with a small blastema and defective neurogenesis and brain formation. These examples demonstrate that anterior and posterior defects are present in both the intact and the regenerating animals. However, differences in the manifestation of these defects are visualized depending on the timeline in which the animals are analyzed (Fig. 2c). Our work suggests that SUMO targets in the posterior regions are more sensitive to changes in their SUMOylation when compared to the anterior counterpart and this is likely the reason for the early posterior defect.

Finally, we provide mechanistic insights behind the cell death-driven regional loss of tissue after *Ubc9*(*RNAi*). Deregulation of Hh pathway by *Ubc9*(*RNAi*) is evident through the steady increase of *Ptc* expression, which is detected early in the phenotype. Previous work has demonstrated that *Ptc* ultimately controls the hedgehog pathway, as high levels of *Ptc* serve to sequester any free Hh and limit the activity of the pathway [55]. Our findings about a role for SUMOylation in regulating Hh signaling are also supported by recent observations in *Drosophila* [56, 57]. Consistently, many members of the Hh pathway are prone to regulation by post-translation modification, such as SUMOylation. For example, Hh stimulates Smo sumoylation by dissociating it from a desumoylation enzyme Ulp1. Sumoylated Smo prevents its ubiquitination and degradation, leading to Smo accumulation on the membrane and elevated Hh pathway activity [56, 57]. Uniquely, our data demonstrate that *Ubc9* is a key regulator of collective cellular decisions such as proliferation and death that are critical for tissue maintenance in the adult body (Fig. 7i). The striking lack of tail regeneration highlights SUMOylation as a region-specific requirement for tissue repair by affecting transcription of Hh genes by regulation of yet to be identified substrate(s). This result is consistent with previous observations in planarians where repression of Hh signaling results in lack of tail regeneration [33, 34]. Nonetheless, it will be interesting to determine whether (1) other mechanisms besides *Ptc* signaling also affect SUMOylation-mediated cell death or (2) if increased *Ptc* expression is involved in regional non-canonical Hh signaling related to cell death. Our findings also highlight the importance of *Ubc9* as an early requirement for neoblasts-driven injury response and suggest that depending on the circumstances SUMOylation may play synergistic/parallel roles or even act as an upstream component of the Hh pathway (Fig. 7i). The *Ubc9* downregulation also extend to *Hh*-mediated impairment of neurogenesis [35], revealing *Ubc9* also controls behavior of neural progenitors and brain function. Hh signaling is also associated with planarian glial cells and future studies will aim to determine whether *Ubc9* loss-of-function affects the function of glial cells through non-canonical Hh signaling. Altogether, our results demonstrate that SUMOylation, in the context of the whole adult body, regulates important aspects of cellular proliferation and cell death at regional and systemic levels (Fig. 7i).

Materials and methods

Planarian culture

Planarian species used in these experiments was *Schmidtea mediterranea* CIW4. The culture was maintained as previously described by [2].

Identification of homologs and phylogenetic analysis

Components of the SUMOylation pathway were identified by BLASTing human SUMO protein sequences into available genomic resources for *S. mediterranea* [58, 59]. Identified sequences underwent a six-frame translation using PFAM and conservation was further confirmed with UNIPROT. The sequences were further verified by Blastn and Blastp in NCBI. The identified sequences were aligned by CLUSTALW with sequences obtained using HomoloGene (http://www.ncbi.nlm.nih.gov/homologene).

Phylogenetic tree for *Ubc9* was constructed using 30 sequences from 30 metazoans and for the SUMO tree we used 31 sequences from 22 metazoans. The sequences were aligned using MAFFT L-INS-I http://mafft.cbrc.jp/alignment/server/ [14]. The alignment was manually adjusted to remove large gaps. Phylogenetic analysis was conducted first by determination of the optimal substitution model for each alignment with ProtTest 2.4 [15]. We constructed maximum likelihood trees in RAxML version 7.3.2 [18], with the appropriate model of protein substitution using the RaxML GUI front end. The best tree and bootsrap proportions were determined by 1000 iterations using Maximum likelihood + Slow bootstrap (100 runs), and PROTGAMMA + LG options using empirical frequencies. Tree images were generated using FigTree (http://tree.bio.ed.ac.uk/software/figtree/), which were then processed using

Adobe Photoshop (http://www.adobe.com/products/photoshopfamily.html).

RNAi experiments

Primers with attb flanking sites were generated for the gene of interest [60]. PCR products were generated using cDNA synthesized from RNA of asexual *S. mediterranea* animals. Thermo Scientific VERSO cDNA synthesis kit was used to make cDNA. The gene was cloned into the pPR244 vector using BP Clonase II kit. The newly generated vector was transformed into NEB5a bacteria and then into HT115 bacteria. HT115 bacteria with the vector was grown in 2XYT media until it reached an OD595 of 0.400. 50 µL of 0.1 M IPTG was added and bacteria were incubated for an additional 4 h. The media was pelleted at 5000 rpm for 5 min and mixed with 25 µL of calf liver and fed to planarians. RNAi feeding times were adjusted for each experiment time.

For *Ubc9*(*RNAi*), planarians were fed UBC9 dsRNA expressing bacteria every 3 days for a total of six feedings. All experiments were performed after 25 days of RNAi starting from the first day of feeding. For double knockdown experiments involving hedgehog and patched RNAi alone, animals were fed with the appropriate dsRNA 8 times every 3 days and then with gfp 6 times every 3 days. For *Ubc9* alone, animals were first fed *gfp* 8 times and then *Ubc9* six times. For *Hh* + *Ubc9* or *Ptc* + *Ubc9*(*RNAi*), animals were fed *Hh* or *Ptc* first and then *Ubc9* after. All animals were fixed at the same time. Same steps were taken to generate animals for the regeneration experiments. For double knockdown experiments involving *Sumo2* and *Sumo3*, 5 ml of bacteria for each gene was grown as before and mixed together before centrifugation. This pellet was once again mixed with 25 µL of calf liver and fed to the planarians. For *Rad51* and *Ubc9* double knockdown, a total of three RAD51 microinjections were administered over three consecutive days and then the animals were fed with Ubc9 dsRNA expressing bacteria 4 times every 3 days.

Whole mount immunofluorescence

Planarians were killed in 5.7% 12 N HCl solution and fixed in Carnoys solution for 2 h on ice. Carnoy's solution was replaced with cold 100% MeOH and animals were placed in −20 °C for 1 h. Worms were bleached overnight in 6% H_2O_2 solution. Worms were then rehydrated in series from 100% MeOH to 100% PBSTx and stained as previously described [9]. Primary antibodies: α-H3p 1:250 (Millipore Cat# 05-817R), α-synapsin, 1:100 (Developmental Studies Hybridoma Bank); and activated caspase-3, 1:500 (Abcam ab13847) [29], RAD51, 1:500 (Abcam ab109107) and Phospho-Histone H2AX 1:1000 (ThemoFisher LF-PA0025) [9]. Similar results were obtained after testing side-by-side the SMED-RAD51 antibody [32] kindly provided by the Sánchez Alvarado/Hawley labs and the commercial RAD51 described above. The results in the manuscript involving RAD51 were obtained with the commercial RAD51 antibody. Secondary antibodies include: Goat anti-mouse Alexa488, 1:400 (Invitrogen Cat# 673781) for α-synapsin, α-arrestin, acetylated tubulin, Goat anti-rabbit Alexa568, 1:800 (Invitrogen Cat# 11036) for H3P, HRP-conjugated Goat anti-rabbit antibody (Millipore Cat# 12-348) with TSA-Alexa568 anti-HRP for caspase-3 (1:2000).

In situ hybridization

Riboprobes for in situ hybridization (ISH) were synthesized using T3 or T7 polymerase (Promega) and digoxigenin labeled ribonucleotide mix (Roche) with specific PCR templates as previously described [9]. Whole-mount ISH (WISH) was performed as previously described [61].

Quantitative real-time PCR

Quantitative real time PCR (qPCR) was performed as previously described [9, 62]. The ubiquitously expressed gene H.55.12e was used as the control. Each individual experiment consisted of triplicates per condition and experiments were independently repeated at least twice. RNA was extracted from anterior and posterior region of animals (> 20 per condition) and converted to cDNA using the Verso cDNA synthesis kit. Gene expression is expressed of fold change in comparison to the control.

Protein extraction and Western blot

Protein studies were performed as previously described [9].

Planarian dissociation

Planarians were amputated, whole or A/P, into small pieces using a razor, suspended in cold calcium, magnesium-free (CMF) media and placed on a rocker for 30 min at 4 °C in the dark. Cells were forced through a 20 micron filter and centrifuged at 1500 rpm followed by resuspension in 1 ml of CMF media before cell counting [23].

Fixation and immunostaining of dissociated cells

Dissociated cells were pipetted onto glass slips and left to anneal for 30 min in the dark. After, the slips were transferred to a glass beaker and fixed in Carnoys solution for 2 h on ice. Carnoys solution was replaced with 100% methanol and transferred to − 20 °C for 1 h. Samples were then rehydrated using mixtures of 75, 50 and 25% Methanol in PBSTx. [2]. After final rehydration with 100% PBSTx

(PBS + 0.3% triton), the cells were blocked in PBST containing bovine albumin serum (BSA) for 4 h RT and primary antibody added overnight: α-RAD51 1:500 (Abcam ab109107). Wash 6 × 10 min in PBSTB and replace with secondary antibody overnight: 1:500 HRP-conjugated Goat anti-rabbit antibody (Millipore Cat# 12-348). Wash 6 × 10 min in PBSTB. Add TSA-Alexa488 in PBSTI 1:1000 for 20 min. Wash 6 × 10 min in PBSTB. Add DAPI (0.1 µg/1 mL) for 15 min and mounted using VECTASHIELD® Mounting Medium.

FACS analysis

FACS analyses were performed as previously described [9, 23].

COMET assay and karyotyping

COMET assay was performed as previously described [9] and karyotyping was performed as previously described [63].

Single-cell sequencing (SCS) data

The *Ubc9* SCS expression analysis was obtained from the planaria single-cell database hosted by the Reddien Lab at the Whitehead Institute for Biomedical Research (https://radiant.wi.mit.edu/app/) [1].

Imaging and data processing

Animal behavior was recorded using a Nikon AZ-100 multizoom microscope and NIS Elements AR 3.2 software. Area measurements were calculated with ImageJ and the difference in animal size were determined as fold change in reference to control group at each time point. Digital pictures were collected using a Nikon AZ-100 multizoom microscope and NIS Elements AR 3.2 software. Brightness and contrast were adjusted with Adobe Photoshop. Neoblasts were counted and normalized to the area (mm^2) using ImageJ. Caspase-3 signal was quantified by measuring levels of fluorescence using NIS element software (Nikon).

Statistical analysis

Data are expressed as mean ± standard error of the mean (SEM) or fold change ± SEM. Statistical analyses were performed in Prism, GraphPad software Inc. (http://www.graphpad.com).

Acknowledgements We thank Edelweiss Pfister for technical assistance and members of the Oviedo Lab for comments on the manuscript. We acknowledge Drs. Marcos Garcia-Ojeda and Anna Beaudin for assistance with FACS analysis and comments on the manuscript. Thanks are also extended to Ulrike Abu-Shach for technical assistance cloning *Ubc9*. The SYNORF antibody was obtained from the Developmental Studies Hybridoma Bank, created by the NICHD of the NIH and maintained at the University of Iowa, Department of Biology. We are grateful to Sánchez Alvarado/Hawley labs for providing a sample of the SMED-RAD51 antibody.

Author contribution statement MT, PGB, AT, LB, and NJO performed research and analyzed data. MT, LB, and NJO wrote the manuscript. All authors read the manuscript, provided comments and approved the final version.

Compliance with ethical standards

Conflict of interest The authors declare no competing or financial interest.

Funding We acknowledge support from University of California Merced and the Israel Science Foundation (ISF 1878/15) and the Israel Cancer Research Fund 14-101-PG to LB. This research was funded by the National Cancer Institute and National Institute of General Medical Sciences of the National Institute of Health, awards CA176114 and GM109372 to NJO.

References

1. Wurtzel O, Cote LE, Poirier A, Satija R, Regev A, Reddien PW (2015) A generic and cell-type-specific wound response precedes regeneration in planarians. Dev Cell 35(5):632–645. https://doi.org/10.1016/j.devcel.2015.11.004
2. Oviedo NJ, Pearson BJ, Levin M, Sánchez Alvarado A (2008) Planarian PTEN homologs regulate stem cells and regeneration through TOR signaling. Dis Model Mech 1(2–3):131–143
3. Owlarn S, Bartscherer K (2016) Go ahead, grow a head! A planarian's guide to anterior regeneration. Regeneration 3(3):139–155. https://doi.org/10.1002/reg2.56
4. Pearson BJ, Sanchez Alvarado A (2008) Regeneration, stem cells, and the evolution of tumor suppression. Cold Spring Harb Symp Quant Biol 73:565–572. https://doi.org/10.1101/sqb.2008.73.045
5. Pellettieri J, Sanchez Alvarado A (2007) Cell turnover and adult tissue homeostasis: from humans to planarians. Annu Rev Genet 41:83–105. https://doi.org/10.1146/annurev.genet.41.110306.130244
6. Roberts-Galbraith RH, Newmark PA (2015) On the organ trail: insights into organ regeneration in the planarian. Curr Opin Genet Dev 32:37–46. https://doi.org/10.1016/j.gde.2015.01.009
7. Tanaka EM, Reddien PW (2011) The cellular basis for animal regeneration. Dev Cell 21(1):172–185. https://doi.org/10.1016/j.devcel.2011.06.016
8. Aboobaker AA (2011) Planarian stem cells: a simple paradigm for regeneration. Trends Cell Biol 21(5):304–311. https://doi.org/10.1016/j.tcb.2011.01.005
9. Peiris TH, Ramirez D, Barghouth PG, Ofoha U, Davidian D, Weckerle F, Oviedo NJ (2016) Regional signals in the planarian body guide stem cell fate in the presence of genomic instability. Development 143(10):1697–1709. https://doi.org/10.1242/dev.131318
10. Epps JL, Tanda S (1998) The Drosophila semushi mutation blocks nuclear import of bicoid during embryogenesis. Current biology: CB 8(23):1277–1280

11. Nowak M, Hammerschmidt M (2006) Ubc9 regulates mitosis and cell survival during zebrafish development. Mol Biol Cell 17(12):5324–5336. https://doi.org/10.1091/mbc.E06-05-0413
12. Lomeli H, Vazquez M (2011) Emerging roles of the SUMO pathway in development. Cell Mol Life Sci 68(24):4045–4064. https://doi.org/10.1007/s00018-011-0792-5
13. Flotho A, Melchior F (2013) Sumoylation: a regulatory protein modification in health and disease. Annu Rev Biochem 82:357–385. https://doi.org/10.1146/annurev-biochem-061909-093311
14. Gareau JR, Lima CD (2010) The SUMO pathway: emerging mechanisms that shape specificity, conjugation and recognition. Nat Rev Mol Cell Biol 11(12):861–871. https://doi.org/10.1038/nrm3011
15. Hay RT (2013) Decoding the SUMO signal. Biochem Soc Trans 41(2):463–473. https://doi.org/10.1042/BST20130015
16. Desterro JM, Thomson J, Hay RT (1997) Ubch9 conjugates SUMO but not ubiquitin. FEBS Lett 417(3):297–300
17. Gong L, Kamitani T, Fujise K, Caskey LS, Yeh ET (1997) Preferential interaction of sentrin with a ubiquitin-conjugating enzyme, Ubc9. J Biol Chem 272(45):28198–28201
18. Johnson ES, Blobel G (1997) Ubc9p is the conjugating enzyme for the ubiquitin-like protein Smt3p. J Biol Chem 272(43):26799–26802
19. Saitoh H, Sparrow DB, Shiomi T, Pu RT, Nishimoto T, Mohun TJ, Dasso M (1998) Ubc9p and the conjugation of SUMO-1 to RanGAP1 and RanBP2. Curr Biol 8(2):121–124
20. Schwarz SE, Matuschewski K, Liakopoulos D, Scheffner M, Jentsch S (1998) The ubiquitin-like proteins SMT3 and SUMO-1 are conjugated by the UBC9 E2 enzyme. Proc Natl Acad Sci USA 95(2):560–564
21. Nacerddine K, Lehembre F, Bhaumik M, Artus J, Cohen-Tannoudji M, Babinet C, Pandolfi PP, Dejean A (2005) The SUMO pathway is essential for nuclear integrity and chromosome segregation in mice. Dev Cell 9(6):769–779. https://doi.org/10.1016/j.devcel.2005.10.007
22. Reddien PW, Oviedo NJ, Jennings JR, Jenkin JC, Sanchez Alvarado A (2005) SMEDWI-2 is a PIWI-like protein that regulates planarian stem cells. Science 310(5752):1327–1330. https://doi.org/10.1126/science.1116110
23. Peiris TH, Garcia-Ojeda ME, Oviedo NJ (2016) Alternative flow cytometry strategies to analyze stem cells and cell death in planarians. Regeneration 3(2):123–135. https://doi.org/10.1002/reg2.53
24. Eisenhoffer GT, Kang H, Sánchez Alvarado A (2008) Molecular analysis of stem cells and their descendants during cell turnover and regeneration in the planarian Schmidtea mediterranea. Cell Stem Cell 3(3):327–339. https://doi.org/10.1016/j.stem.2008.07.002
25. Seufert W, Futcher B, Jentsch S (1995) Role of a ubiquitin-conjugating enzyme in degradation of S- and M-phase cyclins. Nature 373(6509):78–81. https://doi.org/10.1038/373078a0
26. al-Khodairy F, Enoch T, Hagan IM, Carr AM (1995) The Schizosaccharomyces pombe hus5 gene encodes a ubiquitin conjugating enzyme required for normal mitosis. J Cell Sci 108(Pt 2):475–486
27. Meng F, Qian J, Yue H, Li X, Xue K (2016) SUMOylation of Rb enhances its binding with CDK2 and phosphorylation at early G1 phase. Cell Cycle 15(13):1724–1732. https://doi.org/10.1080/15384101.2016.1182267
28. Bellail AC, Olson JJ, Hao C (2014) SUMO1 modification stabilizes CDK6 protein and drives the cell cycle and glioblastoma progression. Nat Commun 5:4234. https://doi.org/10.1038/ncomms5234
29. Beane WS, Morokuma J, Lemire JM, Levin M (2013) Bioelectric signaling regulates head and organ size during planarian regeneration. Development 140(2):313–322. https://doi.org/10.1242/dev.086900
30. Bender CE, Fitzgerald P, Tait SW, Llambi F, McStay GP, Tupper DO, Pellettieri J, Sanchez Alvarado A, Salvesen GS, Green DR (2012) Mitochondrial pathway of apoptosis is ancestral in metazoans. Proc Natl Acad Sci USA 109(13):4904–4909. https://doi.org/10.1073/pnas.1120680109
31. Yin S, Huang Y, Zhangfang Y, Zhong X, Li P, Huang J, Liu D, Songyang Z (2016) SmedOB1 is required for planarian homeostasis and regeneration. Sci Reports 6:34013. https://doi.org/10.1038/srep34013
32. Xiang Y, Miller DE, Ross EJ, Sanchez Alvarado A, Hawley RS (2014) Synaptonemal complex extension from clustered telomeres mediates full-length chromosome pairing in *Schmidtea mediterranea*. Proc Natl Acad Sci USA 111(48):E5159–E5168. https://doi.org/10.1073/pnas.1420287111
33. Yazawa S, Umesono Y, Hayashi T, Tarui H, Agata K (2009) Planarian Hedgehog/Patched establishes anterior-posterior polarity by regulating Wnt signaling. Proc Natl Acad Sci USA 106(52):22329–22334. https://doi.org/10.1073/pnas.0907464106
34. Rink JC, Gurley KA, Elliott SA, Sanchez Alvarado A (2009) Planarian Hh signaling regulates regeneration polarity and links Hh pathway evolution to cilia. Science 326(5958):1406–1410. https://doi.org/10.1126/science.1178712
35. Currie KW, Molinaro AM, Pearson BJ (2016) Neuronal sources of hedgehog modulate neurogenesis in the adult planarian brain. eLife. https://doi.org/10.7554/eLife.19735
36. Auerbach R, Auerbach W (1982) Regional differences in the growth of normal and neoplastic cells. Science 215(4529):127–134
37. Giribet G (2008) Assembling the lophotrochozoan (= spiralian) tree of life. Philos Trans R Soc Lond B Biol Sci 363(1496):1513–1522. https://doi.org/10.1098/rstb.2007.2241
38. Gehrke AR, Srivastava M (2016) Neoblasts and the evolution of whole-body regeneration. Curr Opin Genet Dev 40:131–137. https://doi.org/10.1016/j.gde.2016.07.009
39. Currie KW, Brown DD, Zhu S, Xu C, Voisin V, Bader GD, Pearson BJ (2016) HOX gene complement and expression in the planarian *Schmidtea mediterranea*. EvoDevo 7:7. https://doi.org/10.1186/s13227-016-0044-8
40. Yuan H, Zhou J, Deng M, Liu X, Le Bras M, de The H, Chen SJ, Chen Z, Liu TX, Zhu J (2010) Small ubiquitin-related modifier paralogs are indispensable but functionally redundant during early development of zebrafish. Cell Res 20(2):185–196. https://doi.org/10.1038/cr.2009.101
41. Saracco SA, Miller MJ, Kurepa J, Vierstra RD (2007) Genetic analysis of SUMOylation in *Arabidopsis*: conjugation of SUMO1 and SUMO2 to nuclear proteins is essential. Plant Physiol 145(1):119–134. https://doi.org/10.1104/pp.107.102285
42. Hayashi T, Seki M, Maeda D, Wang W, Kawabe Y, Seki T, Saitoh H, Fukagawa T, Yagi H, Enomoto T (2002) Ubc9 is essential for viability of higher eukaryotic cells. Exp Cell Res 280(2):212–221
43. Yukita A, Hosoya A, Ito Y, Katagiri T, Asashima M, Nakamura H (2012) Ubc9 negatively regulates BMP-mediated osteoblastic differentiation in cultured cells. Bone 50(5):1092–1099. https://doi.org/10.1016/j.bone.2012.02.008
44. Myatt SS, Kongsema M, Man CW, Kelly DJ, Gomes AR, Khongkow P, Karunarathna U, Zona S, Langer JK, Dunsby CW, Coombes RC, French PM, Brosens JJ, Lam EW (2014) SUMOylation inhibits FOXM1 activity and delays mitotic transition. Oncogene 33(34):4316–4329. https://doi.org/10.1038/onc.2013.546
45. Lv X, Pan C, Zhang Z, Xia Y, Chen H, Zhang S, Guo T, Han H, Song H, Zhang L, Zhao Y (2016) SUMO regulates somatic cyst stem cell maintenance and directly targets the Hedgehog pathway in adult Drosophila testis. Development 143(10):1655–1662. https://doi.org/10.1242/dev.130773
46. Tahmasebi S, Ghorbani M, Savage P, Gocevski G, Yang XJ (2014) The SUMO conjugating enzyme Ubc9 is required for inducing

and maintaining stem cell pluripotency. Stem cells 32(4):1012–1020. https://doi.org/10.1002/stem.1600
47. Pelisch F, Sonneville R, Pourkarimi E, Agostinho A, Blow JJ, Gartner A, Hay RT (2014) Dynamic SUMO modification regulates mitotic chromosome assembly and cell cycle progression in *Caenorhabditis elegans*. Nature communications 5:5485. https://doi.org/10.1038/ncomms6485
48. Huang C, Cheng J, Bawa-Khalfe T, Yao X, Chin YE, Yeh ET (2016) SUMOylated ORC2 recruits a histone demethylase to regulate centromeric histone modification and genomic stability. Cell Reports 15(1):147–157. https://doi.org/10.1016/j.celrep.2016.02.091
49. Moschos SJ, Mo YY (2006) Role of SUMO/Ubc9 in DNA damage repair and tumorigenesis. J Mol Histol 37(5–7):309–319. https://doi.org/10.1007/s10735-006-9030-0
50. Shima H, Suzuki H, Sun J, Kono K, Shi L, Kinomura A, Horikoshi Y, Ikura T, Ikura M, Kanaar R, Igarashi K, Saitoh H, Kurumizaka H, Tashiro S (2013) Activation of the SUMO modification system is required for the accumulation of RAD51 at sites of DNA damage. J Cell Sci 126(Pt 22):5284–5292. https://doi.org/10.1242/jcs.133744
51. Kurtzman AL, Schechter N (2001) Ubc9 interacts with a nuclear localization signal and mediates nuclear localization of the paired-like homeobox protein Vsx-1 independent of SUMO-1 modification. Proc Natl Acad Sci USA 98(10):5602–5607. https://doi.org/10.1073/pnas.101129698
52. Ross S, Best JL, Zon LI, Gill G (2002) SUMO-1 modification represses Sp3 transcriptional activation and modulates its subnuclear localization. Mol Cell 10(4):831–842
53. Wu CS, Ouyang J, Mori E, Nguyen HD, Marechal A, Hallet A, Chen DJ, Zou L (2014) SUMOylation of ATRIP potentiates DNA damage signaling by boosting multiple protein interactions in the ATR pathway. Genes Dev 28(13):1472–1484. https://doi.org/10.1101/gad.238535.114
54. Bergink S, Ammon T, Kern M, Schermelleh L, Leonhardt H, Jentsch S (2013) Role of Cdc48/p97 as a SUMO-targeted segregase curbing Rad51-Rad52 interaction. Nat Cell Biol 15(5):526–532. https://doi.org/10.1038/ncb2729
55. Chen Y, Struhl G (1996) Dual roles for patched in sequestering and transducing Hedgehog. Cell 87(3):553–563
56. Ma G, Li S, Han Y, Li S, Yue T, Wang B, Jiang J (2016) Regulation of smoothened trafficking and hedgehog signaling by the SUMO pathway. Dev Cell 39(4):438–451. https://doi.org/10.1016/j.devcel.2016.09.014
57. Zhang J, Liu Y, Jiang K, Jia J (2017) SUMO regulates the activity of Smoothened and Costal-2 in Drosophila Hedgehog signaling. Sci Reports 7:42749. https://doi.org/10.1038/srep42749
58. Robb SM, Gotting K, Ross E, Sanchez Alvarado A (2015) SmedGD 2.0: the Schmidtea mediterranea genome database. Genesis 53(8):535–546. https://doi.org/10.1002/dvg.22872
59. Brandl H, Moon H, Vila-Farre M, Liu SY, Henry I, Rink JC (2016) PlanMine–a mineable resource of planarian biology and biodiversity. Nucleic Acids Res 44(D1):D764–D773. https://doi.org/10.1093/nar/gkv1148
60. Reddien PW, Bermange AL, Murfitt KJ, Jennings JR, Sánchez Alvarado A (2005) Identification of genes needed for regeneration, stem cell function, and tissue homeostasis by systematic gene perturbation in planaria. Dev Cell 8(5):635–649
61. Pearson BJ, Eisenhoffer GT, Gurley KA, Rink JC, Miller DE, Sanchez Alvarado A (2009) Formaldehyde-based whole-mount in situ hybridization method for planarians. Dev Dyn 238(2):443–450. https://doi.org/10.1002/dvdy.21849
62. Peiris TH, Ramirez D, Barghouth PG, Oviedo NJ (2016) The Akt signaling pathway is required for tissue maintenance and regeneration in planarians. BMC Dev Biol 16:7. https://doi.org/10.1186/s12861-016-0107-z
63. Guedelhoefer OCT, Sanchez Alvarado A (2012) Amputation induces stem cell mobilization to sites of injury during planarian regeneration. Development 139(19):3510–3520. https://doi.org/10.1242/dev.082099